ELSEVIER

Journal of Electron Spectroscopy and Related Phenomena 123 (2002) 287–302

JOURNAL OF ELECTRON SPECTROSCOPY and Related Phenomena

www.elsevier.com/locate/elspec

Non-dipole electron impact spectroscopy of a common local anesthetic: Generalized oscillator strengths of valence, Cl 2p and C 1s pre-edge transitions of chloroethane

X.W. Fan, K.T. Leung*

Department of Chemistry, University of Waterloo, Waterloo, Ontario, Canada N2L 3G1

Received 30 October 2001; received in revised form 23 January 2002; accepted 25 January 2002

This paper is dedicated to Professor C.E. Brion on the occasion of his 65th birthday.

Abstract

Angle-resolved electron energy loss spectroscopy at 2.5 keV impact energy has been used to determine absolute generalized oscillator strengths (GOSs) of discrete transitions in the pre-edge regions of the valence, Cl 2p and C 1s shells of chloroethane as functions of energy loss and momentum transfer. A new lowest-lying preionization-edge energy-loss feature at 7.2 eV has been clearly identified at a non-zero momentum transfer. The corresponding GOS profile is found to have a shape characteristic of non-dipole transitions that can be attributed to electronic excitations from nonbonding Cl 3p initial-state orbitals (4a″ and 13a′) to antibonding σ^*_{C-Cl} final-state orbital (14a′). The GOS profiles of the other low-lying valence-shell and Cl 2p and C 1s pre-edge features are found to have maximum intensity at zero momentum transfer, generally consistent with the spectral assignments to dipole-allowed transitions involving final-state Rydberg orbitals. Differences in and between the GOS profiles for the valence-shell and these inner-shell pre-edge features in C_2H_5Cl are identified. Although no discernible secondary extrema can be found in any of the inner-shell GOS profiles, subtle differences can be observed and are consistent with the proposed assignments. The present GOS results for C_2H_5Cl are compared with the available GOS data reported for other mono-chlorides, including CF_3Cl and CHF_2Cl.

Keywords: Angle-resolved electron energy loss spectroscopy; GOS profiles; Valence and inner shells

1. Introduction

Electron scattering has evolved in the past three decades as one of the most powerful tools for investigating the electronic structure of matter and electron-induced processes. In a typical inelastic electron scattering process, the transfer of energy and momentum from the incident electron to the atomic or molecular target can produce both dipole and non-dipole excitations from its electronic ground state (M) to an excited state (M^*),

$$e^-(E_0, \mathbf{k_0}) + M \rightarrow e^-(E_0 - E, \mathbf{k}) + M^*, \quad (1)$$

*Corresponding author. Tel.: +1-519-888-4567 ext. 5826; fax: +1-519-746-0435.
E-mail address: tong@uwaterloo.ca (K.T. Leung).

0368-2048/02/$ – see front matter
PII: S0368-2048(02)00028-2

where E_0 (or $E_0 - E$) and $\mathbf{k}_0$ (or $\mathbf{k}$) are the kinetic energy and momentum of the incident (or scattered) electron, respectively, and E is the energy loss. The magnitude of the momentum transfer $\mathbf{K}$ ($=\mathbf{k}_0 - \mathbf{k}$) is connected to the scattering angle, θ, by $K^2 = k_0^2 + k^2 - 2\,k_0\,k\cos\theta$. According to the Bethe theory [1], the scattering cross section for a sufficiently fast collision is related to the generalized oscillator strength (GOS) of the corresponding electronic transition. First introduced to electron scattering by Bethe [1] and later elaborated in detail by Inokuti [2], the GOS, $f(K, E)$, is defined as:

$$f(K,E) = \frac{E}{K^2}\left|\left\langle \Psi_n \left| \sum_{j=1}^{N} \exp(i\,\mathbf{K}\cdot\mathbf{r}_j) \right| \Psi_0 \right\rangle\right|^2, \qquad (2)$$

where Ψ_0 and Ψ_n are the N-electron electronic wavefunctions of the initial (ground) and final states respectively, and $\mathbf{r}_j$ is the position of the jth electron with respect to the centre-of-mass of the target. The GOSs measured at different K values are therefore related qualitatively to the corresponding Fourier-transform components of the overlap function between the initial-state and final-state wavefunctions. For small K, the GOS can be expanded into a power series [3,4]:

$$\begin{aligned} f(K,E) &\approx \epsilon_1^2 + (\epsilon_2^2 - 2\epsilon_1\epsilon_3)|\mathbf{K}|^2 \\ &\quad + (\epsilon_3^2 - 2\epsilon_2\epsilon_4 + 2\epsilon_1\epsilon_5)|\mathbf{K}|^4 + \cdots \\ &= f_0 + f_1|\mathbf{K}|^2 + f_2|\mathbf{K}|^4 + \cdots, \end{aligned} \qquad (3)$$

where the multipole transition moment is given by

$$\epsilon_m = \frac{1}{m!}\left\langle \Psi_n \left| \sum_{j=1}^{N} \left(\frac{\mathbf{K}}{|\mathbf{K}|}\cdot\mathbf{r}_j\right)^m \right| \Psi_0 \right\rangle.$$

The GOS converges to the dipole oscillator strength, f_0, as K approaches zero [5]. The f_1 term contains information related to the quadrupole transition probability. Study of the angular dependence of the GOS of a bound state therefore offers a means to obtain information about the qualitative nature of the transition, which is particularly useful for the characterization of non-dipole phenomena. In effect, GOS measurement can provide a detailed 'mapping' of the overlap function in momentum space, which can in turn be used as an effective feedback for theoretical modelling of the excited state [6].

Angle-resolved electron energy loss spectroscopy (EELS) offers a powerful technique for 'complete' determination of the excited states, including the dipole-allowed and the optically inaccessible non-dipole states [7]. Over three decades ago, Lassettre and coworkers pioneered the use of angle-resolved EELS for accurate determination of absolute dipole OS by extrapolating precise GOS measurement to the optical limit [5]. Moreover, the so-called pseudo-photon experiments by Brion, van der Wiel and coworkers [8] involve 'near-zero' forward-angle electron scattering at high impact energy, in which case the 'distant' collision of the electron effectively simulates the interaction due to a dipole field. Even given the generally lower resolving power when compared with modern synchrotron-radiation photoabsorption spectroscopy, zero-angle EELS technique (i.e., at a negligible momentum transfer) [9] has two fundamental advantages over photoabsorption methods for obtaining the dipole OS. These are the collection of precise absolute cross section (oscillator strength) data over a wide energy range without performing an 'absolute' experiment and the avoidance of the difficulties associated with the use of the Beer–Lambert law [10]. On the other hand, GOS measurement as a function of the scattering angle or, equivalently, the momentum transfer (i.e. away from the dipole limit) provides additional and often unique information about the nature of the electronic transitions and of the electron scattering process itself. In particular, experiments by Bonham and coworkers [11] and Lassettre and coworkers [3] have demonstrated the use of these K-dependent studies as a powerful means for investigating dipole-forbidden and other multipole excitation phenomena. New non-dipole transitions have been discovered by using angle-resolved EELS in the valence-shell (including O_2, CO, NO, CO_2, N_2O [12], N_2 [13,14], C_2H_2 [15], benzene [16], and *p*-difluorobenzene [17]) and inner-shell regions (including N 1*s* in N_2 [18,19], NO and N_2O [19], C 1*s* in CO [20], CO_2 [21], C_2H_2 [22,23], C_2H_4 and C_6H_6 [23], S 2p [24,25] and S 2s [26] in SF_6). In the past several years, angle-resolved EELS has been used in our laboratory to study the electronic structures of the valence and inner shells of a number of polyatomic molecules, particularly chlorofluorocarbons (CFCs), $CF_{4-n}Cl_n$ ($n = 0$–4) [27–30], and their chlorofluorohydrocarbon (CFHC)

homologs, $CHF_{3-m}Cl_m$ ($m = 0$–3) [31–33]. A current review of our work and this particular area has been given by Leung [34]. Very recently, we have extended our investigation to electronic excitations in the outer-core shells of Ar [35] and the autoionization resonances in Ar [36] and He [37], as well as the shape resonance structures in such cage-like molecules as SiF_4 [38,39] and SF_6 [24,40].

Chloroethane is commonly used as a local anesthetic to control pain associated with minor surgical procedures, muscle tension, contusion, etc. It is among the 189 chemicals designated in the 1990 Clean Air Act to be regulated by the U.S. Environmental Protection Agency. Given that the methyl group ($-CH_3$) is isoelectronic with the fluorine atom, study of the ligand substitution effect of a fluorine atom by a methyl group may provide insights into selected electronic transitions and the corresponding electronic structures of the excited states. In our earlier angle-resolved EELS studies of CFCs [27–30] and CFHCs [31–33], the lowest-lying preionization-edge transitions are found to invariably involve excitation from a non-bonding Cl 3p orbital (highest occupied molecular orbital or HOMO) to an antibonding σ^*_{C-Cl} orbital (lowest unoccupied molecular orbital or LUMO). Furthermore, these HOMO→LUMO transitions involve predominantly non-dipole excitation, which could potentially provide a low-lying dissociative channel for the Cl atom. The lack of symmetry in chloroethane (with a C_s symmetry) also provides an opportunity to examine the importance of molecular symmetry on these low-lying pre-edge transitions. In the case of inner-shell transitions, chloroethane offers a unique system to evaluate atomic-site-specific and other core-level relaxation effects in GOS profiles for transitions originating from initial states localized at three different atomic centres (Cl and two C). The sensitivity of the GOS profiles for probing local chemical environment is of special interest to the fundamental understanding of the inner-shell transitions. Unlike the smaller alkyl halides, there are only a very limited number of studies on the electronic structure of chloroethane of relevance to the present work. In 1974, Raymonda et al. compared the vacuum ultraviolet absorption spectra of chloromethane with a series of larger chloroalkanes and reported the optical OSs of the three lowest-lying preionization-edge bands [41]. Later in 1978, Hitchcock and Brion reported zero-angle EELS spectra for the C 1s and Cl 2p and 2s regions in a series of chloromethanes and chloroethane [42]. The present work reports new measurement of absolute GOS profiles for some of the more prominent transitions in the valence and inner shells reported in the earlier studies [41,42] and further characterizes the nature (and assignments) of these transitions by examining the angular dependence of their OSs. These results are compared with our earlier work on CFCs [27–30] and CFHCs [31–33].

2. Experimental method

The apparatus and the experimental procedure used for the present angle-resolved EELS study have been described in detail elsewhere [35]. Briefly, a collimated electron beam was accelerated to 2.5 keV impact energy and crossed with a gas jet expanded from a nozzle (0.5 mm diameter) positioned at 1 cm above the collision centre. Electrons scattered with an energy loss E at a scattering angle θ (from the forward direction) were analyzed using a hemispherical energy analyzer equipped with a seven-element input lens, and the corresponding intensity of the scattered electron is proportional to the differential cross section $d^2\sigma/d\Omega\ dE$. Angle-resolved EELS spectra of the sample gas introduced to the center of the collision cell (sample spectra) were collected at a series of θ angles (corresponding to different momentum transfers) sequentially in repetitive scans. An identical set of EELS spectra of the sample gas introduced outside the collision cell at the same pressure ($1–2\times10^{-5}$ Torr) were recorded in the same energy loss and angular ranges (ambience spectra), after each measurement of the sample spectra. Contributions from the ambient gas were removed by subtracting the corresponding ambience spectra from the sample spectra after appropriate normalization. This correction of the ambience contribution is essential to assuring precise GOS measurement especially for inner-shell and other transitions with low cross sections.

For high-energy electron collisions, the influence of the incident electron upon the target can be regarded as a sudden and impulsive encounter.

Under these conditions (and after the EELS spectra have been relatively normalized to one another), the differential cross section can be converted (in the first Born approximation) to the differential GOS, $df(K, E)/dE$, by using the Bethe–Born formula (in Rydberg atomic units) [2]:

$$\frac{df(K,E)}{dE} = \frac{k_0}{k} K^2 \frac{E}{4} \frac{d^2\sigma}{d\Omega\, dE} \quad (4)$$

where $d\Omega$ corresponds to the detection solid angle. The GOS for any constant value of K can also be made absolute independently using the Bethe sum rule [2]:

$$\int \frac{df(K,E)}{dE} dE = N \quad (5)$$

where N is the total number of electrons in the target. In the Bethe-sum-rule normalization procedure, the intensity of the relative GOS obtained at a particular momentum transfer was first numerically integrated over a sampling energy loss range of 170 eV. The remaining intensity of the valence shell above 170 eV for C_2H_5Cl was estimated by integration of a fitted function $B(E) = a/E^{1.5} + b/E^{2.5} + c/E^{3.5}$ from 170 eV to infinity, where the empirical constants a, b, and c were obtained by curve-fitting $B(E)$ to the experimental data in the energy loss range of 70–170 eV. The sum of these two integrated intensities was then normalized to the integrated oscillator strength of 20.71, which corresponds to the total number of valence-shell electrons (20), plus an appropriate correction of the contribution due to Pauli-excluded transitions from the inner shells (0.71) [43,44].

For angle-dependent studies that involve finite K values, Lassettre and coworkers [5] pointed out that the GOS for a bound-state excitation can be expanded as an even power series of momentum transfer (the so-called Lassettre series):

$$f(K,E) = \frac{1}{(1+x)^6} \sum_{n=0}^{m} f_n \left(\frac{x}{1+x}\right)^n \quad (6)$$

where

$$x = \frac{K^2}{\left(\sqrt{2I} + \sqrt{2|I-W|}\right)^2},$$

I is the ionization potential, and W is the excitation energy of the discrete transition. The integer m ($=3$ in the present expansion) is chosen according to the amount of available data points and the accessible experimental range of momentum transfer. In the limit when K approaches zero, the GOS approaches the dipole OS, f_0. The original Lassettre series has been used quite successfully for quantitative estimate of the dipole OS by extrapolating the measured GOS data to zero momentum transfer [5]. The other parameters f_n in the Lassettre series are related to linear combinations of the respective multipole matrix elements (Eq. (3)) [4]. In the present work, the Lassettre series is used to provide semi-quantitative characterization of the nature of the underlying transitions.

Chloroethane (99.7% purity) was purchased from Aldrich and used without further purification. Our spectrometer was operated routinely with an energy resolution of 0.8 eV full-width at half-maximum and an angular resolution of 0.2° half-angle. The angular scale was calibrated periodically by comparing the measured GOS of the pre-ionization bound ($1s \rightarrow 2p$ and $1s \rightarrow 2s$) transitions of He with reliable theoretical calculations, while the energy loss scale could be calibrated in situ with an energy loss spectrum of a known background gas (such as N_2) [25,35]. No geometrical correction was found to be necessary for the small experimental angular range and the high impact energy employed in the present work. An energy loss spectrum of N_2 over an extended energy range (up to the N 1s region) has also been collected and found to be in good accord with the literature data [45]. No correction due to the lens transmission effect was found to be necessary because of the high impact energy used. The accuracy of the absolute GOS data reported in the present work was estimated to be 25% [45].

3. Results and discussion

3.1. Overview of the electronic structure of valence and inner shells in C_2H_5Cl

Chloroethane is a 34-electron system with C_s molecular symmetry. In accord with data from ultraviolet [46] and X-ray photoelectron spectroscopy [47,48] and Penning ionization studies [49], the

single-electron configuration for the ground electronic state of C_2H_5Cl can be written as:

Core orbitals: $\underbrace{1a'^2}_{Cl\ 1s}\ \underbrace{2a'^2 3a'^2}_{C\ 1s}\ \underbrace{4a'^2}_{Cl\ 2s}\ \underbrace{5a'^2 6a'^2 1a''^2}_{Cl\ 2p}$

Valence orbitals: $\underbrace{7a'^2 8a'^2 9a'^2}_{\text{Inner-valence}}\ \underbrace{2a''^2 10a'^2 11a'^2 3a''^2 12a'^2 13a'^2 4a''^2}_{\text{Outer-valence}}$

Fig. 1 shows a typical EELS spectrum for the valence-shell and the Cl 2p and 2s, as well as the C 1s regions collected at 2.5° from the forward scattering direction. The vertical ionization potentials for the removal of the outer-valence molecular orbitals (MOs), the energies for the main ionic states of the inner-valence orbitals, and the term values for the unoccupied virtual MOs and Rydberg orbitals are summarized in Table 1 [47,49]. Several prominent pre-edge states have been identified and they are found to be generally consistent with the photoabsorption features below 11.2 eV observed by Raymonda et al. [41] and with the near-edge features of Cl 2p and 2s and C 1s shells reported by Hitchcock and Brion [42]. The observed minor differences in the relative intensities could be attributed to differences in the scattering angle and the energy resolution. It should be noted that Fig. 1 represents the first absolute spectrum that provides absolute OS data over an extended energy loss range up to 305 eV. The valence-shell preionization-edge region (at 2.5°) is generally featureless but with notable shoulders corresponding to discrete electronic excitation and Rydberg transitions in the rising edge converging towards the first ionization threshold. Above the ionization threshold, the absorption spectrum follows the 'generic' profile of a rising band followed by a falling tail. Due to the complexities in this region, excitation spectroscopy such as photoabsorption and EELS would not be the best tool to decipher the multitude of electronic excitation and ionization structures. The present work therefore concentrates on the preionization-edge discrete excitation features and their assignments are given in more detail in Section 3.2. Similarly, several broad features are notable below the ionization edges of Cl $2p_{3/2}$ at 206.0 eV and Cl $2p_{1/2}$ at 207.6 eV as well as C_1 1s at 291.1 eV and C_2 1s at 292.1 eV (C_1 and C_2 denote the methane-like carbon and methyl chloride-like carbon, respectively). Unlike the cage-like molecules (such as CCl_4 [30], SiF_4 [36], and SF_6 [40]), no intense peaks attributable to σ* shape resonances can be observed in C_2H_5Cl. The inner-shell pre-edge features in C_2H_5Cl correspond mostly to Rydberg transitions converging to the respective ionization edges. Further details of their assignments are discussed in Section 3.3.

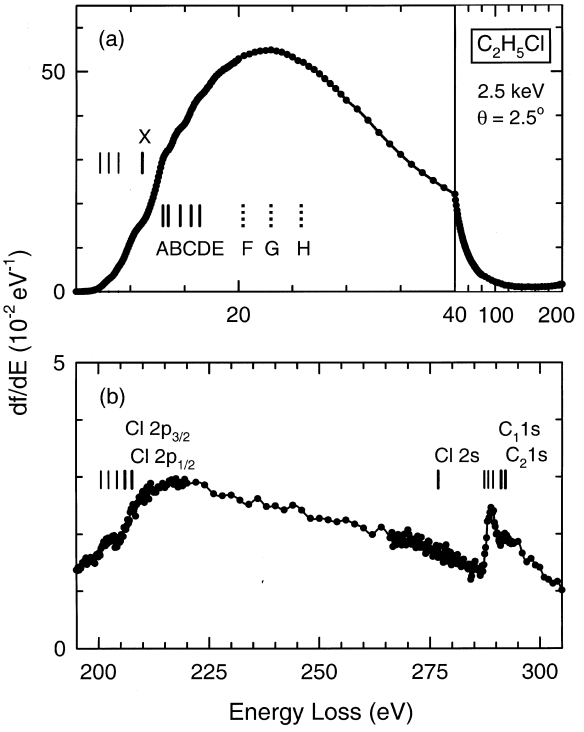

Fig. 1. Absolute electron energy loss spectra of the valence shell (upper panel) and Cl 2p, Cl 2s and C 1s shells (Lower panel) of C_2H_5Cl recorded at 2.5° and 2.5 keV impact energy. The vertical ionization potentials for the outer-valence ionic states: X(4a″ or 13a′)$^{-1}$, A(12a′)$^{-1}$, B(3a″)$^{-1}$, C(11a′)$^{-1}$, D(10a′)$^{-1}$ and E(2a″)$^{-1}$ and the energies for the main-line inner-valence ionic states F(9a′)$^{-1}$, G(8a′)$^{-1}$ and H(7a′)$^{-1}$ are obtained from the photoelectron data [47,49]. The ionization potentials of the Cl $2p_{3/2}$, $2p_{1/2}$ and 2s as well as the C_1 1s and C_2 1s edges are 206.0, 207.6, 276.8, 291.1 and 292.1 eV respectively [42].

Fig. 2 shows the EELS spectra of the valence shell of C_2H_5Cl collected in steps of 0.5° from 1.0° to 8.5° in the form of a Bethe surface plot. These angle-resolved EELS spectra have been obtained relatively normalized to one another and made absolute using

Table 1
Experimental vertical ionization potentials (IPs) of the occupied valence orbitals and term values of the unoccupied virtual and Rydberg orbitals in C_2H_5Cl

Occupied orbital	IP (eV) Ref. [47,49]	Unoccupied orbital	Term value (eV)[a] This work[b]	Ref. [42] C1 2p Scheme A[c]	Ref. [42] Cl 2p Scheme B[c]	Ref. [42] C 1s[d]
4a″, 13a′ (HOMO's)	11.1	5p				1.8 (1.5)
12a′	13.0	5s		3.7 (3.4)		
3a″	13.5	4p	2.2	3.7 (5.3)	3.7 (3.4)	2.9 (2.8)
11a′	14.6	4s	3.1	5.4 (5.3)	3.7 (5.3)	3.8 (3.9)
10a′	15.6	14a″ (LUMO)	3.9		5.4 (5.3)	(4.8)
2a″	16.4					
9a′	20.4					
8a′	23.0					
7a′	25.8					

[a] The term values of the virtual orbitals derived from the inner-shell transitions are always larger than those from valence-shell transitions due to a larger relaxation effect in the inner shells [51].

[b] These values correspond to the term values obtained from the valence-shell preionization-edge features and are essentially the same as those that could be derived from the photoabsorption data of Raymonda et al. [41].

[c] Hitchcock and Brion [42] proposed two possible assignments, Scheme A and Scheme B, based on their Cl 2p zero-angle EELS spectra. The values without and with round parentheses correspond to term values derived from Cl $2p_{3/2}$ and Cl $2p_{1/2}$, respectively. The ionization edges for Cl $2p_{3/2}$ and Cl $2p_{1/2}$ are located at 206.0 eV and 207.6 eV, respectively.

[d] The values without and with round parentheses correspond to term values derived from the 1s shells of C_1 (methane-like carbon) and C_2 (methyl chloride-like carbon), respectively [42]. The ionization edges for C_1 1s and C_2 1s are located at 291.1 eV and 292.1 eV, respectively.

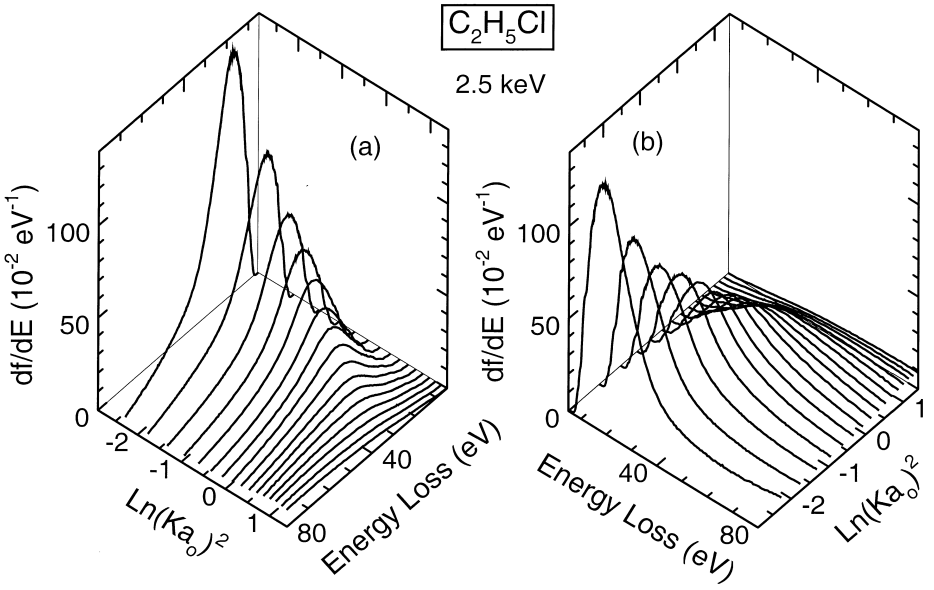

Fig. 2. Bethe surface of the valence shell of C_2H_5Cl determined at 2.5 keV impact energy. Absolute angle-resolved electron energy loss spectra were collected in steps of 0.5° from 1.0° to 8.5° repetitively in sequence scans and have been made absolute by applying the Bethe-sum-rule normalization procedure to the 1.5° spectrum.

the Bethe sum rule. In the framework of the first Born scattering theory, the Bethe surface is a three-dimensional representation of the GOS as a function of energy loss and the logarithm to the base e of the square of the momentum transfer. Because it contains information about the nature of the inelastic electron scattering process with an atom or a molecule, the Bethe surface can be used for analyzing such quantities as stopping power, total inelastic scattering cross section, the Compton profile and polarizability [2]. The Bethe surface can be generally divided into two kinematical domains: dipole-scattering and impact-scattering. For 'distant' collisions, which are mainly governed by dipole interaction, the corresponding dipole-scattering domain of small momentum transfer and energy loss exhibits generally discrete 'optical' features found in the valence shell (Fig. 2b). For 'close' collisions, the corresponding impact-scattering domain of large momentum transfer and energy loss reveals a weak broad ridge that disperses to a higher energy loss with increasing momentum transfer (Fig. 2a). This ridge is the result of momentum conservation in the inelastic electron-molecule collision and becomes the well-known Bethe ridge in the Born approximation. The energy dispersion of this ridge with respect to K is generally related to manifestation of different Fourier-transform components of the overlap density between the initial-state and final-state wave functions [2].

Because the methyl group is isoelectronic to a fluorine atom, it is of interest to compare the Bethe surface of CH_3CH_2Cl (Fig. 2) with the available angle-resolved EELS data for other monochlorinated CFC and CFHC molecules, particularly CF_3Cl [29] and CHF_2Cl [32]. (Unfortunately, absolute EELS data for CH_2FCl is not currently available.) The Bethe surfaces of these molecules are expected to be similar to one another because the primary difference is related to successive replacement of hydrogen by fluorine (or fluorine-equivalent ligand such as the methyl group in the case of C_2H_5Cl). The overall spectral envelope of the preionization-edge features in C_2H_5Cl resembles more closely to that of CHF_2Cl [32] than CF_3Cl [29], which generally reflects the similarities (or differences) in the nature of the electronic structures (and molecular symmetry) in these molecules. Furthermore, the spectral intensity of the maximum of the Bethe surface for C_2H_5Cl (i.e., near the ionization threshold) is notably higher and more concentrated in the lower energy-loss region than CH_2FCl and CF_3Cl, suggesting a more delocalized spatial distribution of the valence-shell electron densities in C_2H_5Cl relative to the other molecules. Evidently the presence of the methyl group in C_2H_5Cl is producing a lower average charge density in the valence shell, generally favouring 'distance' collisions (i.e., the dipole-scattering region with a smaller momentum transfer).

3.2. Preionization-edge valence-shell features in C_2H_5Cl

Fig. 3 shows selected angle-resolved EELS spectra of the valence-shell region of C_2H_5Cl in the energy loss range of 5–15 eV collected at 1.0°, 3.0°, 5.0°, and 8.0°, which correspond to momentum transfers of 0.24, 0.71, 1.18, and 1.89 a.u. at 15 eV energy loss, respectively. These spectra have been Bethe–Born-corrected and normalized by the Bethe sum rule as discussed above. The angle-resolved EELS spectra clearly reveal the emergence of a weak feature with its intensity peaking at a non-zero scattering angle (Fig. 3c). This non-dipole feature is located at 7.2 eV, i.e. at an energy that is 0.8 eV below the onset of the predominantly dipole-allowed Rydberg states observed in the 1° spectrum (Fig. 3a). Except for this lowest-lying feature, the overall spectral intensity of the entire pre-ionization-edge structure becomes reduced with increasing momentum transfer, which is generally characteristic of the predominantly dipole-allowed nature of the underlying transitions. The nature of the transitions assigned to these low-lying preionization-edge features can be quantified in more detail by examining their respective GOS profiles. In particular, the preionization-edge features have been fitted with five Gaussian peaks at 7.2 eV (feature 1), 8.0 eV (feature 2), 8.9 eV (feature 3), 9.9 eV (feature 4), and 11.1 eV (ionization threshold of the ground ionic state). Only the three lowest-lying peaks are used for estimating the corresponding GOS profiles, while the peaks at 9.9 eV and 11.1 eV are used to simulate the contribution from the on-set of the ionization edge for the ground ionic state. The widths of the Gaussian line-shapes have been estimated from the high-resolution ultra-

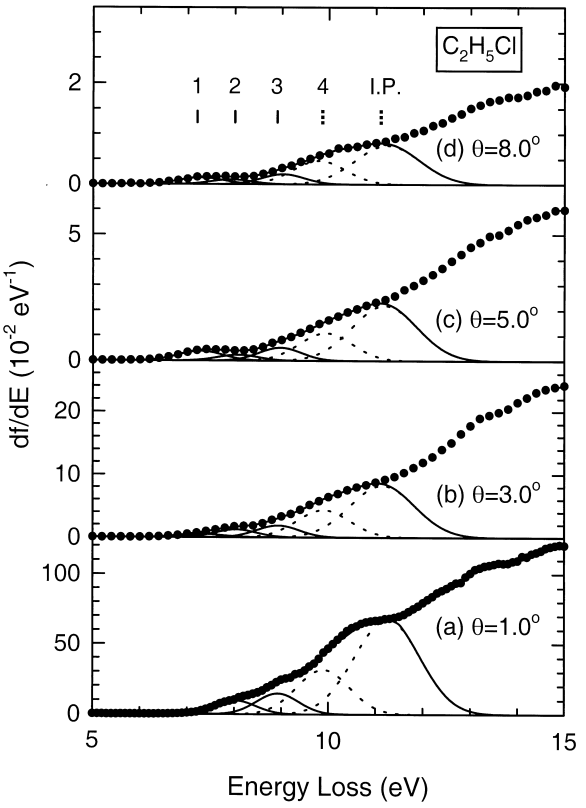

Fig. 3. Absolute angle-resolved electron energy loss spectra of the valence shell of C_2H_5Cl measured at (a) 1.0°, (b) 3.0°, (c) 5.0°, and (d) 8.0°. Five Gaussian line-shapes with the appropriate line-widths are used to estimate the intensities of the pre-ionization-edge structures at 7.2 eV (feature 1), 8.0 eV (feature 2), 8.9 eV (feature 3), 9.9 eV (feature 4), and 11.1 eV in a curve-fitting procedure, with the latter two peaks used to simulate the structure near the ionization potential (I.P.).

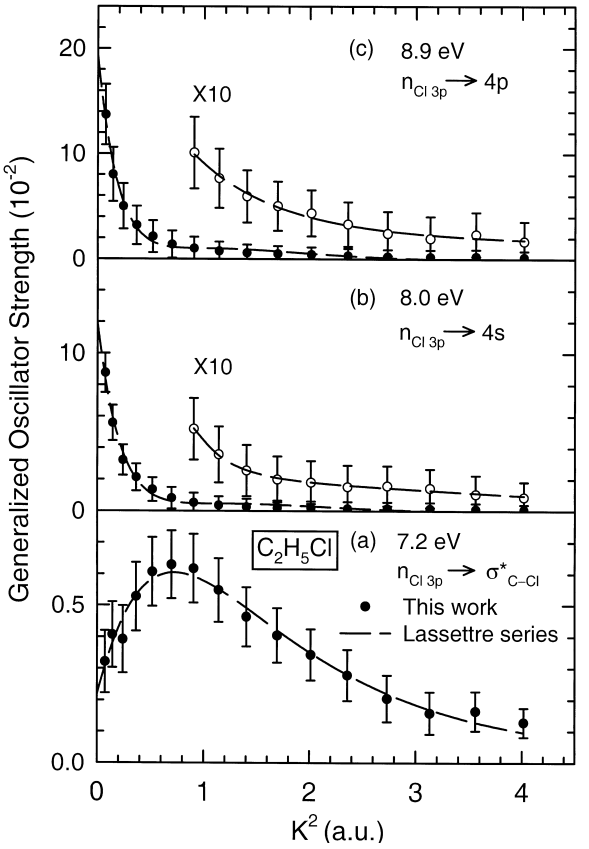

Fig. 4. Absolute generalized oscillator strength as a function of momentum transfer (K) squared for the preionization-edge features at (a) 7.2 eV, (b) 8.0 eV, and (c) 8.9 eV in C_2H_5Cl. The dashed lines correspond to semiempirical fits using the Lassettre series.

violet absorption spectrum reported by Raymonda et al. [41], after taking our instrumental energy resolution into account. The GOSs of these features are determined from the areas under the respective Gaussian peaks in the absolute angle-resolved EELS spectra collected at different scattering angles, and the resulting experimental GOS profiles are shown in Fig. 4. Semiempirical fitting to the experimental GOS profiles by using the Lassettre series (Eq. (6)) is also used to extract not only the dipole OS by extrapolation to $K = 0$ but also other coefficients that are related to linear combinations of various multipole transition matrix elements [3,4]. These f_n coefficients, along with the proposed assignments by Raymonda et al. [41], are given in Table 2.

By comparing the photoabsorption spectra of methyl chloride and C_2H_5Cl, Raymonda et al. assigned the lowest-lying features semiempirically as transitions from nonbonding to antibonding σ* orbitals ($n \rightarrow \sigma^*$) based largely on their very weak spectral intensities [41]. This assignment is confirmed definitively for the first time in the present work by the GOS profile of the lowest-lying feature at 7.2 eV in C_2H_5Cl shown in Fig. 4a, which clearly depicts the characteristic non-dipole shape with a relative maximum located at non-zero momentum transfer. As was previously found for the HOMO→LUMO transitions in CFCs [27–30] and

Table 2
Tentative assignments and the Lassettre coefficients of the observed preionization-edge valence-shell features in the angle-resolved EELS spectra of C_2H_5Cl. The term values (in units of eV) for the final-state orbitals are given in square parentheses

Feature	Energy loss (eV)	Assignment Ref. [41]	f_0 [a]	f_1/f_0	f_2/f_0	f_3/f_0
1	7.2	(13a′, 4a″)→14a′	0.0022	30.6	91.3	−106.9
		[3.9]	±16%	±20%	±50%	±75%
2	8.0	(13a′, 4a″)→4s	0.120	−12.4	54.8	−71.8
		[3.1]	±4%	±10%	±17%	±24%
3	8.9	(13a′, 4a″)→4p	0.193	−12.1	54.6	−70.4
		[2.2]	±4%	±11%	±18%	±26%

[a] The dipole oscillator strengths for features 1, 2 and 3 reported by Raymonda et al. [41] are 0.02, 0.23 and 0.42, respectively.

CFHCs [31–33], simple MO calculations show that the (degenerate) initial-state orbitals (HOMOs), 13a′ and 4a″, for the lowest-lying transitions in C_2H_5Cl consist essentially of nonbonding Cl 3p orbitals ($n_{Cl\ 3p}$) while the final-state orbital (LUMO), 14a′, corresponds to a C–Cl antibonding σ* orbital (σ^*_{C-Cl}). Because the overlap between the initial-state and final-state orbital wavefunctions occurs mostly at the Cl site, the transition moment of this type of $n_{Cl\ 3p}\rightarrow\sigma^*_{C-Cl}$ electronic transitions is therefore expected to resemble that of a p-to-p transition in a Cl atom, which readily gives rise to the characteristic quadrupole-allowed shape of the GOS profile. Based on symmetry consideration alone, all the possible electronic transitions in a molecule belonging to the C_s point group are formally dipole-allowed. Specifically, however, the 13a′→14a′ and the 4a″→14a′ transitions are both electric-dipole-allowed and quadrupole-allowed. The small dipole OS value f_0 for the $n_{Cl\ 3p}\rightarrow\sigma^*_{C-Cl}$ transitions in C_2H_5Cl obtained by extrapolation of the GOS profile to zero momentum transfer using the Lassettre fit, as shown in Table 2, is consistent with the non-dipole nature of the assigned transitions. As shown in Eq. (3), the f_n coefficients in the Lassettre series expansion can be related to linear combinations of the respective multipole transition matrix elements and can in principle be used to characterize the nature of the transition itself. It has been shown by Huo that the f_1 term is related to the difference of the square of the quadrupole matrix element and the product of the dipole and octupole matrix elements [4]. For dipole or octupole-dominated transitions, the f_2 coefficient (in the present expansion to $n = 3$) is found to have a positive sign while the odd coefficients, f_1 and f_3, are negative. (The dipole OS f_0 is always positive.) In our earlier work, we have shown that the higher-order coefficients of a quadrupole-allowed transition appear to reverse in sign relative to the corresponding coefficients for a dipole-allowed transition [24,31]. The positive sign of the f_1 term is therefore indicative of predominantly quadrupole-allowed transitions. However, the dipole OS value ($f_0 = 0.0022$) for the $n_{Cl\ 3p}\rightarrow\sigma^*_{C-Cl}$ transitions in C_2H_5Cl obtained in the present work is not in agreement with the optical value (0.02) reported by Raymonda et al. [41]. The intensities of many of the bands for methyl chloride reported by Raymonda et al. [41] were also found to differ substantially from the absolute zero-angle EELS spectra obtained by Olney et al. [50]. The differences were attributed partially to different spectral resolutions and mainly to line saturation effects encountered in the optical photoabsorption experiment [50]. In the present case of C_2H_5Cl, even after applying a similar multiplicative correction factor of 0.33, as employed by Olney et al. [50], to the OS values reported by Raymonda et al. [41], a substantial difference remains for the $n_{Cl\ 3p}\rightarrow\sigma^*_{C-Cl}$ transitions. We believe that the remaining discrepancy could be due to difficulty in estimating the peak area for the very weak non-dipole feature (particularly from the residual background) in the photoabsorption experiment [41].

Despite the general similarity, subtle differences can be found between the GOS profiles of the $n_{Cl\ 3p}\rightarrow\sigma^*_{C-Cl}$ transitions in C_2H_5Cl and those in CF_3Cl and CHF_2Cl [31]. (The GOS profiles of the $n_{Cl\ 3p}\rightarrow\sigma^*_{C-Cl}$ transitions in the latter two molecules have been found to be very similar to each other [31].) In particular, both the location of the relative

maximum at $K^2 \sim 0.7$ a.u. and the half-width of $K^2 \sim 2.1$ a.u. for the GOS profile of the $n_{Cl\ 3p} \rightarrow \sigma^*_{C-Cl}$ transitions in C_2H_5Cl are found to be smaller than the location of the relative maximum at $K^2 \sim 1.0$ a.u. (1.0 a.u.) and half width of $K^2 \sim 2.9$ a.u. (2.7 a.u.) for the corresponding GOS profile in CF_3Cl (CHF_2Cl) [31]. Given the GOS maximum of the $n_{Cl\ 3p} \rightarrow \sigma^*_{C-Cl}$ transitions in C_2H_5Cl (~0.006) is approximately half of that of the corresponding transitions in CF_3Cl and CHF_2Cl (0.013–0.014), the GOS integrated over the lower momentum-transfer region of the $n_{Cl\ 3p} \rightarrow \sigma^*_{C-Cl}$ transitions in C_2H_5Cl therefore appears to be smaller than that in CF_3Cl and CHF_2Cl. These differences in magnitudes and shapes, reflecting the different distributions of the momentum-transfer components, underline the differences in the nature of the connecting initial states and final states involved in the electronic excitation processes (at different energy losses). It has been shown in our earlier work that the $n_{Cl\ 3p} \rightarrow \sigma^*_{C-Cl}$ transitions in CF_3Cl and CHF_2Cl [31] as well as other CFC [27–30] and CFHC molecules [31–33] that contain non-dipole interactions could lead to the dissociation of the C–Cl bond. We hypothesize that the predissociative nature of the HOMO→LUMO transitions may also apply in the case of C_2H_5Cl. These common dissociation processes in chlorinated compounds are clearly of interest to the understanding of photochemical and electron-induced processes in the upper atmosphere and in plasma-related industrial applications.

Figs. 4b and 4c show the GOS profiles of the features at 8.0 eV (feature 2) and 8.9 eV (feature 3), which have been attributed to $n_{Cl\ 3p} \rightarrow 4s$ and $n_{Cl\ 3p} \rightarrow 4p$ Rydberg transitions, respectively, by Raymonda et al. [41] (Table 2). The $n_{Cl\ 3p}$ initial-state orbitals correspond to the degenerate 13a′ and 4a″ MOs consisting mainly of Cl 3p atomic characters as discussed above. Evidently, the strong maximum at $K = 0$ and the general shape of these two GOS profiles are characteristic of predominantly dipole-allowed transitions. Both GOS profiles have half-widths of $K^2 \sim 0.15$ a.u. and do not contain any discernible secondary extrema. The marked reduction of coherent features such as secondary GOS maxima and minima from the Rydberg transitions in CF_3Cl [29] to those in CHF_2Cl [32] and finally complete extinction of secondary GOS extrema in C_2H_5Cl are likely caused by disruption from the higher-symmetry structure to the C_s symmetry, preventing strong molecular diffraction effect from taking place. The sharpness of these GOS profiles is consistent with the dipole-allowed Rydberg transitions observed earlier, e.g. those in CF_3Cl [29] and CHF_2Cl [32], which is in accord with the similar f_n parameters obtained for this type of valence-shell Rydberg transitions (shown in Table 2). However, as noted earlier, the dipole OS values (f_0) obtained for features 2 and 3 are smaller than the reported values by Raymonda et al. [41], which are believed to be incorrect as discussed also by Olney et al. [50]. It is also of interest to note that the sum of dipole OSs for the $n_{Cl\ 3p} \rightarrow 4s$ and $n_{Cl\ 3p} \rightarrow 4p$ Rydberg transitions in C_2H_5Cl (0.313) is quite similar to those of the same transitions in CF_3Cl (0.29) (Fig. 10a in Ref. [29]) and CHF_2Cl (0.31) (Fig. 8a in Ref. [32]). This similarity suggests that at low momentum transfer the ‘localized’ excitation of the nonbonding Cl 3p MOs, regardless of the resident molecular structure, proceeds largely via two excitation channels involving transitions to the 4s and 4p Rydberg orbitals. At higher momentum transfer, however, additional non-dipole excitation mechanisms of the nonbonding Cl 3p MOs become accessible via the antibonding σ^*_{C-Cl} MOs.

3.3. Pre-edge transitions in the Cl 2p and C 1s shells of C_2H_5Cl

Figs. 5 and 6 show selected absolute EELS spectra of C_2H_5Cl for the Cl 2p region at 2.5°, 4.0°, 6.0°, and 8.0° (corresponding to momentum transfers of 0.82, 1.09, 1.51, and 1.94 a.u. at 210 eV energy loss, respectively) and the C 1s region at 1.5°, 3.0°, 5.0°, and 8.0° (corresponding to momentum transfers of 0.89, 1.07, 1.60, and 2.01 a.u. at 295 eV energy loss, respectively). The background from the valence-shell contribution has been appropriately removed from these inner-shell spectra, which are automatically normalized on an absolute scale because the entire EELS spectra (from the valence shell up to 305 eV) were collected in a self-normalized fashion as discussed previously. Several well-defined pre-edge features at 200.6 eV (feature 1), 202.3 eV (feature 2), and 204.2 eV (feature 3) in Fig. 5 and at 287.3 eV (feature 1), 288.2 eV (feature 2), and 289.3 eV

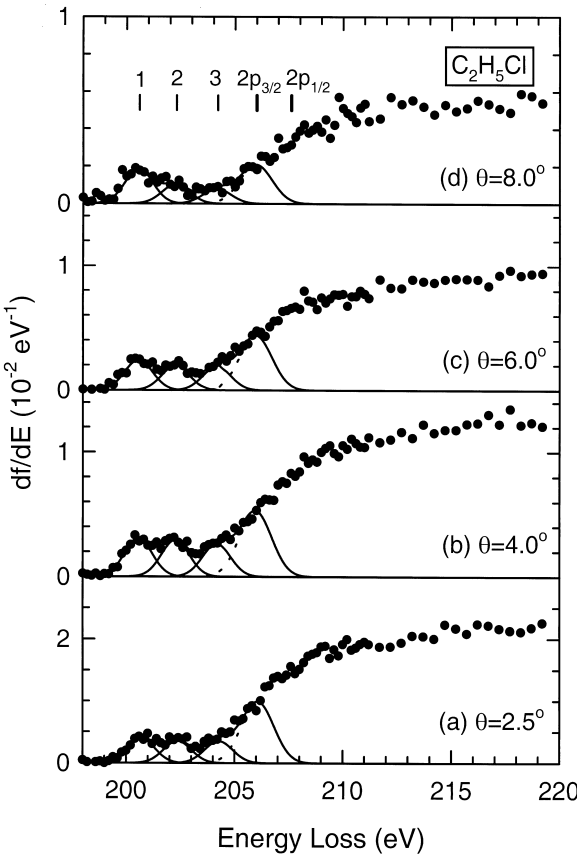

Fig. 5. Absolute angle-resolved electron energy loss spectra for the Cl 2p region of C_2H_5Cl measured at (a) 2.5°, (b) 4.0°, (c) 6.0°, and (d) 8.0°. Intensities from the valence shell have been removed from the background. Three Gaussian line-shapes with the appropriate line-widths are used in a curve-fitting procedure to estimate the intensities of the structures at 200.6 eV (feature 1), 202.3 eV (feature 2), and 204.2 eV (feature 3), with the fourth peak at 206.0 eV used to simulate the on-set of the Cl $2p_{3/2}$ ionization edge.

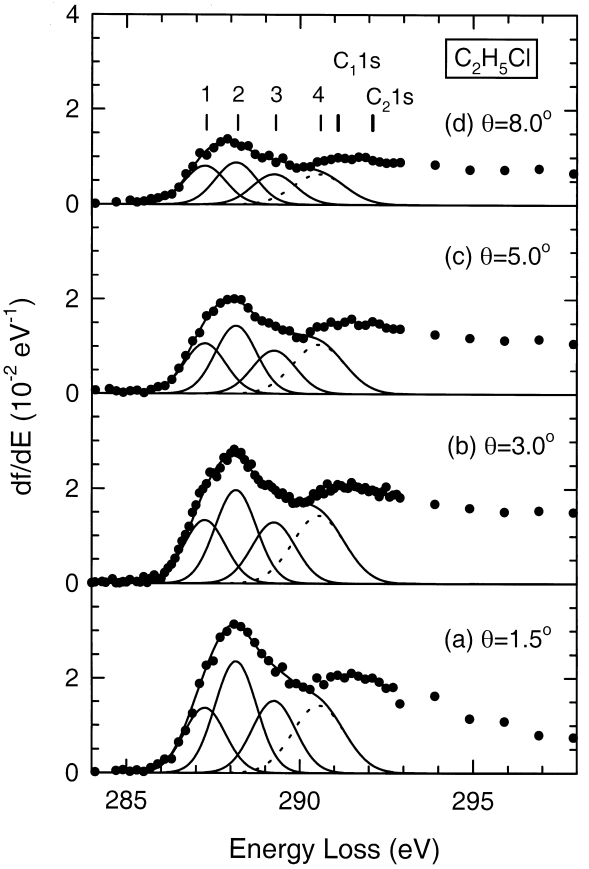

Fig. 6. Absolute angle-resolved electron energy loss spectra for the C 1s region of C_2H_5Cl measured at (a) 1.5°, (b) 3.0°, (c) 5.0°, and (d) 8.0°. Intensities from the valence shell have been removed from the background. Three Gaussian line-shapes with the appropriate line-widths are used in a curve-fitting procedure to estimate the intensities of the structures at 287.3 eV (feature 1), 288.2 eV (feature 2), and 289.3 eV (feature 3), with the fourth peak at 290.6 eV used to simulate the on-set of the C_1 1s and C_2 1s ionization edges at 291.1 and 292.1 eV, respectively.

(feature 3) in Fig. 6 are identified by a Gaussian fitting procedure, employing the respective natural line widths appropriate for the two inner-shell regions as estimated from the zero-angle EELS spectra of Hitchcock and Brion [42]. As with the deconvolution procedure used for the valence shell, additional peaks at 206.0 eV and 290.6 eV are used to simulate the on-sets of the ionization edges for Cl $2p_{3/2}$ at 206.0 eV and Cl $2p_{1/2}$ at 207.6 eV and for C_1 1s at 291.1 eV and C_2 1s at 292.1 eV, respectively. The Cl 2p and C 1s pre-edge structures (Figs. 5a and 6a) are of similar magnitude to each other but are significantly weaker (by at least an order of magnitude) than the valence-shell structure (Fig. 3a). In accord with the inner-shell transitions studied by angle-resolved EELS to date [30], the changes in the overall spectral intensities in the Cl 2p and C 1s pre-edge regions with momentum transfer are generally more gradual and over a more extended momentum-transfer range than that of the valence shell. Evidently, the spectral intensities of the Cl 2p and C 1s pre-edge features shown in Figs. 5 and 6 are found to decrease with increasing momentum trans-

fer, which is generally characteristic of the predominantly dipole-allowed nature of the underlying transitions. Except for a general reduction in the overall intensity, there is no discernible difference in the general shape of the energy loss structure at the larger scattering angles in the respective inner-shell regions. Table 3 summarizes the early assignments for these Cl 2p and C 1s pre-edge features made by Hitchcock and Brion [42], which are largely based on transitions to Rydberg orbitals with the additional σ^*_{C-Cl} orbital, 14a′.

Fig. 7 shows the GOS profiles of the three fitted Cl 2p pre-edge features in C_2H_5Cl, estimated from the areas under the respective Gaussian line-shapes identified in Fig. 5. These GOS profiles are also fitted semiempirically with the Lassettre series to obtain the respective dipole OSs and other f_n coefficients shown in Table 3. These coefficients may be used to qualitatively describe the overall shapes of the GOS profiles for dipole-allowed and non-dipole transitions dominated by a strong $K=0$ component. In particular, the coefficients f_1 and f_2 play an important role in the lower momentum-transfer region ($K^2<2$ a.u.) while the coefficients f_2 and f_3 govern the higher momentum-transfer part. In the present case, the dipole OSs (f_0) of these pre-edge Cl 2p features are found to be small and all the respective f_n parameters are of similar magnitude to one another. The magnitudes of the f_1/f_0 and f_2/f_0 ratios for the GOS profiles of feature 1 are notably larger than those of the corresponding ratios for the GOS profiles of features 2 and 3 (Table 3), reflecting the slightly different shape for feature 1.

The gradual descending shapes from its maximum at $K=0$ with increasing momentum transfer for the GOS profiles of the Cl 2p pre-edge features (Fig. 7) are generally consistent with the spectral assignments that these Cl 2p pre-edge features are dominated by dipole-allowed transitions. In particular, except for the first feature at 200.6 eV (feature 1) that has been attributed to a Cl $2p_{3/2}\rightarrow 14a'$ transition in addition to the Cl $2p_{3/2}\rightarrow 4s$ Rydberg transition, the remaining two features are assigned primarily to Cl 2p transitions with Rydberg orbitals as the final states. The main features of a GOS profile can be understood qualitatively in terms of Fourier-transform components of the spatial overlap between the initial-state and the final-state wavefunctions Eq. (2). In the case of inner-shell transitions, the initial-state wavefunction is localized at the respective atomic centre. The GOS profile is therefore sensitive to the bonding environment in the 'small' spatial region of

Table 3
Tentative assignments and the Lassettre coefficients of the observed pre-edge features in the Cl 2p and C 1s shells of the angle-resolved EELS spectra of C_2H_5Cl. The term values (in units of eV) for the final-state orbitals are given in square parentheses

Feature	Energy loss (eV)	Assignment[a] Ref. [42]	f_0	f_1/f_0	f_2/f_0	f_3/f_0
1	200.6	Cl $2p_{3/2}\rightarrow 4s$ [5.4]	0.0096	−22.2	341.9	−1686.3
		(Cl $2p_{3/2}\rightarrow 14a'$)[b] [5.4]	±4%	±14%	±19%	±23%
2	202.3	Cl $2p_{3/2}\rightarrow 4p$ [3.7]	0.0076	−15.3	201.8	−1172.1
		(Cl $2p_{3/2}\rightarrow 4s$)[b] [3.7]	±10%	±42%	±62%	±62%
		Cl $2p_{1/2}\rightarrow 4s$ [5.3]				
		(Cl $2p_{1/2}\rightarrow 14a'$)[b] [5.3]				
3	204.2	Cl $2p_{1/2}\rightarrow 5s$ [3.4]	0.0083	−19.1	288.4	−1734.2
		(Cl $2p_{1/2}\rightarrow 4p$)[b] [3.4]	±9%	±31%	±38%	±35%
1	287.3	C_1 $1s\rightarrow 4s$ [3.8]	0.0269	−14.6	287.1	−2186.3
		C_2 $1s\rightarrow 14a'$ [4.8]	±9%	±55%	±67%	±63%
2	288.2	C_1 $1s\rightarrow 4p$ [2.9]	0.0525	−22.8	281.8	−1126.9
		C_2 $1s\rightarrow 4s$ [3.9]	±4%	±16%	±29%	±52%
3	289.3	C_1 $1s\rightarrow 5p$ [1.8]	0.0367	−24.8	403.5	−2441.5
		C_2 $1s\rightarrow 4p$ [2.8]	±6%	±20%	±28%	±31%

[a] The ionization edges for Cl $2p_{3/2}$ and Cl $2p_{1/2}$ are located at 206.0 eV and 207.6 eV, respectively, while those for the 1s shells of C_1 (methane-like carbon) and C_2 (methyl chloride-like carbon) are located at 291.1 eV and 292.1 eV, respectively.

[b] The Cl 2p assignments without and with the round parentheses correspond to Schemes A and B proposed by Hitchcock and Brion [42], respectively.

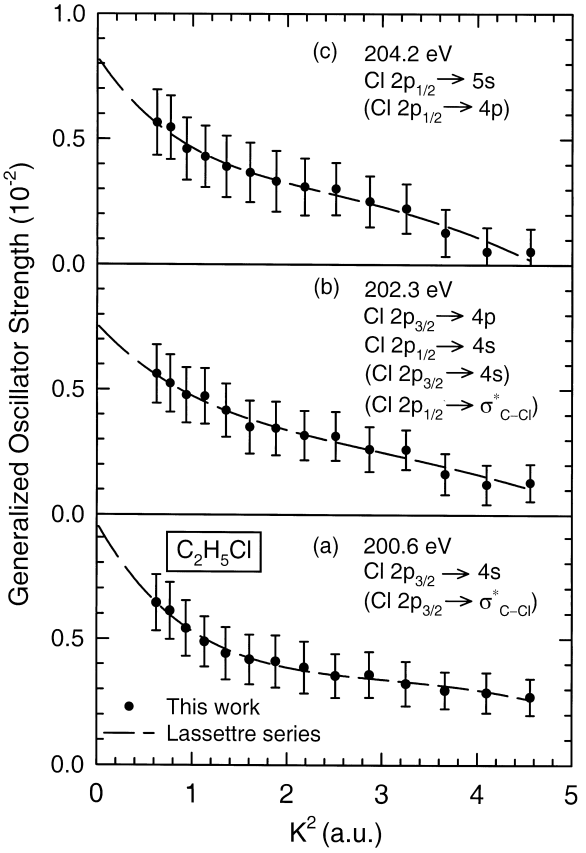

Fig. 7. Absolute generalized oscillator strength as a function of momentum transfer (K) squared for the Cl 2p pre-edge features at (a) 200.6 eV, (b) 202.3 eV, and (c) 204.2 eV in C_2H_5Cl. The dashed lines correspond to semiempirical fits using the Lassettre series. The Cl 2p assignments without and with the round parentheses correspond to Schemes A and B proposed by Hitchcock and Brion [42], respectively.

the unoccupied excited-state wavefunction at the respective atomic site. While the GOS profile of the lowest-lying Cl 2p pre-edge feature (Fig. 7a) is very similar to those of the higher lying pre-edge features (Figs. 7b and 7c), i.e., all with a monotonically decreasing GOS profile with increasing momentum transfer, the higher momentum-transfer part of the GOS profile is found to be discernibly more intense (i.e., with a 'flatter' GOS profile) than those of the other two features. This notable difference could be due to the underlying non-dipole contribution from the Cl $2p_{3/2}\rightarrow 14a'$ transition, which like the $n_{Cl\ 3p}\rightarrow 14a'$ transition is expected to exhibit a GOS profile with a relative maximum at non-zero momentum transfer. In particular, since the 14a′ orbital consists predominantly of σ^*_{C-Cl} overlap with strong s and p components at both the Cl and C sites, the corresponding dipole-dominated (p→s) and non-dipole (p→p) components could therefore give rise to the GOS maxima at the K origin and non-zero K, respectively. The latter (p→p) quadrupole component should be similar to that observed for the GOS profile of the $n_{Cl\ 3p}\rightarrow 14a'$ (HOMO→LUMO) transition, which contains a dominant peak with maximum at $K^2\approx 0.7$ a.u. (Fig. 4a). Indeed, maxima have been found at $K=0$ and $K^2\sim 1.2$ a.u. in the GOS profiles of the analogous Cl $2p_{3/2}\rightarrow\sigma^*_{C-Cl}$ and Cl $2p_{1/2}\rightarrow\sigma^*_{C-Cl}$ transitions in our earlier work on CF_3Cl [30]. In the present case, any relative GOS maximum at nonzero momentum transfer is likely obscured by the strongly dipole-allowed GOS contribution from the Cl $2p_{3/2}\rightarrow 4s$ Rydberg transition (Fig. 7a), thereby producing only a minor effect in the GOS profile.

Feature 2 at 202.3 eV (Fig. 7b) is assigned to an admixture of Cl $2p_{3/2}\rightarrow 4p$ and Cl $2p_{1/2}\rightarrow 4s$ (as in Scheme A involving only Rydberg transitions) or of Cl $2p_{3/2}\rightarrow 4s$ and Cl $2p_{1/2}\rightarrow 14a'$ (as in Scheme B with mixed electronic and Rydberg excitations), or both [42]. With the exception of the Cl $2p_{1/2}\rightarrow 14a'$ transition, all of the proposed contributing Rydberg transitions are dipole-allowed. The lack of any discernible secondary maximum would suggest that the contribution from the Cl $2p_{1/2}\rightarrow 14a'$ transition does not play a prominent role. Feature 3 at 204.2 eV (Fig. 7c) is attributed to only Rydberg transitions: Cl $2p_{1/2}\rightarrow 5s$ and/or Cl $2p_{1/2}\rightarrow 4p$, both of which would exhibit GOS profiles characteristic of dipole-allowed excitations. Consistent with our earlier inner-shell GOS studies [30], the present work shows that the GOS profiles for the Cl 2p (and C 1s) pre-edge excitation transitions are considerably broader than those for the valence-shell transitions, which are found to contain sharper variations (as shown in Fig. 4).

Fig. 8 shows the GOS profiles of the low-lying C 1s pre-edge features. In particular, only the feature at 287.3 (Fig. 8a) has been attributed to an admixture of both C_1 1s→4s Rydberg and C_2 1s→14a′ electronic excitations, while the features at 288.2 eV (Fig. 8b) and at 289.3 eV (Fig. 8c) have been assigned as

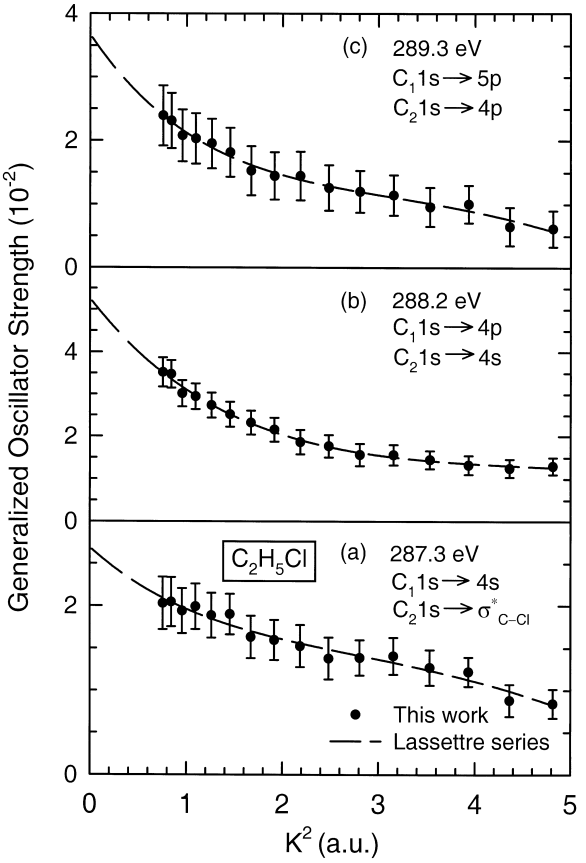

Fig. 8. Absolute generalized oscillator strength as a function of momentum transfer (K) squared for the C 1s pre-edge features at (a) 287.3 eV, (b) 288.2 eV, and (c) 289.3 eV in C_2H_5Cl. The dashed lines correspond to semiempirical fits using the Lassettre series.

admixtures of Rydberg transitions involving C_1 1s→4p and C_2 1s→4s, and C_1 1s→5p and C_2 1s→4p, respectively [42]. Evidently, the shapes of these C 1s GOS profiles are all characteristic of dipole-dominated transitions. Unlike the GOS profiles of the higher-lying C 1s pre-edge features with a somewhat sharper peak at low momentum transfer (Figs. 8b and 8c), the GOS profile of the lowest-lying C 1s pre-edge feature evidently has a more monotonically linear shape (Fig. 8a). The 'flatter' shape of the GOS profile of the lowest-lying C 1s pre-edge feature is reflected more quantitatively by the smallest magnitude of its f_1 parameter in the Lassettre fit with respect to those of the other two GOS profiles (Table 3). This notable difference may be the result of the underlying contribution from the C_2 1s→14a′ electronic excitation, unlike the other features with contributions from Rydberg transitions only. It is also of interest to note that the GOS profile of the lowest-lying C 1s pre-edge feature (Fig. 8a) is also found to be similar in shape to that of C 1s→11a_1 feature in CF_3Cl (an analogous C 1s→σ^*_{C-Cl} feature). The apparent similarity is clearly related to the similarities in the final-state orbitals, both of which consist of σ* density overlap of the C–Cl bond, and it also suggests that the remaining contribution from the C_1 1s→4s Rydberg transition may not play a major role.

The GOS profiles for these C 1s excitations remain fairly intense even at K^2~5 a.u. and are found to be relatively stronger than those of the Cl 2p transitions at higher momentum transfer. This behaviour is consistent with the deeper core holes from which these transitions originate, where the higher K components correspond to 'close' collisions that occur near the nuclear centre. A more systematic study of the GOS profiles of these inner-shell transitions involving a larger database would be useful to a more quantitative analysis. It is clear, however, that the subtle differences found in the GOS profiles do reflect the intricacy of the underlying transitions and the nature of the connecting initial and final states. There is a serious need for quantitative calculations and theoretical investigations of these inner-shell processes.

4. Concluding remarks

Absolute GOS profiles of selected pre-edge structures of the valence and Cl 2p and C 1s shells in C_2H_5Cl have been determined using angle-resolved EELS at 2.5 keV impact energy. In particular, a well-defined lowest-lying preionization-edge energy-loss feature at 7.2 eV is clearly resolved at a non-zero momentum transfer. The corresponding GOS profile for this lowest-lying preionization-edge, (13a′, 4a″)→ 14a′ (HOMO→LUMO) transitions is found to have a shape that is characteristic of quadrupole-allowed transitions. While this type of transitions is both dipole and quadrupole-allowed

according to symmetry arguments, the corresponding GOS profile with its maximum oscillator strength observed at $K^2 \sim 0.7$ a.u. gives convincing evidence that these $n_{Cl} \rightarrow \sigma^*_{C-Cl}$ transitions are predominantly due to quadrupole interactions. The other excitations in the valence shell involve Rydberg orbitals in their final states, and all appear to have a monotonically descending profile with its maximum at $K = 0$ but a different degree of descending slope, generally indicative of dipole-dominated transitions. The GOS profiles of these Rydberg excitations are found to be quite similar to the corresponding GOS profiles involving analogous Rydberg transitions in other monochloride homologs, CF_3Cl [29] and CHF_2Cl [32]. However, these GOS profiles in C_2H_5Cl do not contain any discernible secondary extrema that are commonly found in more cage-like molecules [27–30], which illustrates the general sensitivity of GOS profiles to the molecular structure and symmetry of the underlying transitions.

The Cl 2p and C 1s pre-edge regions are dominated by predominantly dipole-allowed Rydberg transitions. Although the corresponding GOS profiles of these inner-shell pre-edge features are found to have a shape generally characteristic of dipole-allowed transitions, minor differences in the descending shape ('flatness') can be observed. The GOS profiles of these inner-shell transitions are found to be considerably broader than the valence-shell transitions in general. The present work shows that despite the similarity in the general appearance of the measured GOS profiles, their differences underline the nature of the contributing transitions. Further experimental GOS investigations with a higher energy resolution and especially new complementary theoretical studies involving more quantitative GOS analysis are of great interest to advancing our current understanding of the intricate electronic structures of saturated chlorinated compounds. Inner-shell excitations to low-lying excited states below the ionization continuum offer new opportunities for studying non-dipole excited-state spectroscopy and atomic-site-specific electron-induced chemistry, as well as other fundamental effects such as electron correlation. This and other continual efforts from other groups will provide a more comprehensive 'absolute' GOS database to foster new insights into the electronic structures of polyatomic molecules that can be distinctly probed by angle-resolved electron scattering methods.

Acknowledgements

This work was supported by the Natural Sciences and Engineering Research Council of Canada.

References

[1] H. Bethe, Ann. Phys. 5 (1930) 325;
H. Bethe, Z. Physik 76 (1932) 293.
[2] M. Inokuti, Rev. Mod. Phys. 43 (1971) 297.
[3] E.N. Lassettre, A. Skerbele, in: D. Williams (Ed.), Methods of Experimental Physics, Vol. 3 (Part B), Academic, New York, 1974, p. 868, Chapter 7.2.
[4] W.M. Huo, J. Chem. Phys. 71 (1979) 1593.
[5] E.N. Lassettre, J. Chem. Phys. 43 (1965) 4479;
M.A. Dillon, E.N. Lassettre, J. Chem. Phys. 62 (1975) 2373;
See also: M.A. Dillon, M. Inokuti, Z.W. Wang, Rad. Res. 102 (1985) 151.
[6] J.B. Foresman, M. Head-Gordon, J.A. Pople, M.J. Frisch, J. Phys. Chem. 96 (1992) 135.
[7] R.A. Bonham, J.S. Lee, R. Kennerly, W. St. John, Adv. Quant. Chem. 2 (1978) 1.
[8] A. Hamnett, W. Stoll, G. Branton, C.E. Brion, M.J. van der Wiel, J. Phys. B. 9 (1976) 945.
[9] T.N. Olney, N.M. Cann, G. Cooper, C.E. Brion, Chem. Phys. 223 (1997) 59.
[10] W.F. Chan, G. Cooper, C.E. Brion, Phys. Rev. A 44 (1991) 186.
[11] R.A. Bonham, in: C.R. Brundle, A.D. Baker (Eds.), Electron Spectroscopy: Theory, Techniques and Applications, Vol. 3, Academic, New York, 1979, p. 127.
[12] J.S. Lee, J. Chem. Phys. 67 (1977) 3998.
[13] A. Skerbele, E.N. Lassettre, J. Chem. Phys. 53 (1970) 3806;
J.S. Lee, T.C. Wong, R.A. Bonham, J. Chem. Phys. 63 (1975) 1643;
N. Oda, T. Osawa, J. Phys. B 14 (1981) L563;
G.G.B. de Souza, C.A. Lucas, in: M.J. Coggiola, D.L. Heustis, R.P. Saxon (Eds.), ICPEAC Book of Abstracts, Palo Alto, 1985, North-Holland, Amsterdam, 1985, p. 252;
E. Fainelli, R. Camilloni, G. Petrocelli, G. Stefani, Nuovo Cimento D 9 (1987) 33.
[14] R.S. Barbieri, R.A. Bonham, Phys. Rev. A 45 (1992) 7929, and references therein.
[15] A.C.A. Souza, G.G.B. de Souza, Phys. Rev. A 38 (1988) 4488.
[16] K.N. Klump, E.N. Lassettre, Chem. Phys. Lett. 51 (1977) 99.
[17] K.N. Klump, E.N. Lassettre, J. Chem. Phys. 68 (1978) 3511.
[18] D.A. Shaw, G.C. King, F.H. Read, D. Cvejanovic, J. Phys. B 15 (1982) 1785.

[19] R. Camilloni, E. Fainelli, G. Petrocelli, G. Stefani, J. Phys. B 20 (1987) 1839.
[20] J.T. Francis, N. Kosugi, A.P. Hitchcock, J. Chem. Phys. 101 (1994) 11429.
[21] H.M. Boechat Roberty, C.E. Bielschowsky, G.G.B. de Souza, Phys. Rev. A 44 (1991) 1694.
[22] M.P. de Miranda, C.E. Bielschowsky, H.M. Boechat Roberty, G.G.B. de Souza, Phys. Rev. A 49 (1994) 2399.
[23] J.T. Francis, C. Enkvist, S. Lunell, A.P. Hitchcock, Can. J. Phys. 72 (1994) 879.
[24] J.F. Ying, C.P. Mathers, K.T. Leung, Phys. Rev. A 47 (1993) R5.
[25] J.T. Francis, C.C. Turci, T. Tyliszczak, G.G.B. de Souza, N. Kosugi, A.P. Hitchcock, Phys. Rev. A 52 (1995) 4665; C.C. Turci, J.T. Francis, T. Tyliszczak, G.G.B. de Souza, A.P. Hitchcock, Phys. Rev. A 52 (1995) 4678.
[26] A.P. Hitchcock, I.G. Eustatiu, J.T. Francis, C.C. Turci, J. Electron Spectrosc. Relat. Phenomen. 88–91 (1998) 77.
[27] J.F. Ying, K.T. Leung, J. Chem. Phys. 100 (1994) 7120.
[28] J.F. Ying, C.P. Mathers, K.T. Leung, H.P. Pritchard, C. Winstead, V. McKoy, Chem. Phys. Lett. 212 (1993) 289.
[29] J.F. Ying, K.T. Leung, J. Chem. Phys. 101 (1994) 8333.
[30] J.F. Ying, K.T. Leung, J. Chem. Phys. 101 (1994) 7311, and references therein.
[31] J.F. Ying, K.T. Leung, J. Chem. Phys. 100 (1994) 1011.
[32] J.F. Ying, K.T. Leung, J. Chem. Phys. 105 (1996) 2188.
[33] J.F. Ying, K.T. Leung, Phys. Rev. A 53 (1996) 1476.
[34] K.T. Leung, J. Elec. Spect. Relat. Phenom. 100 (1999) 237.
[35] X.W. Fan, K.T. Leung, Phys. Rev. A 62 (2000) 62703.
[36] X.W. Fan, K.T. Leung, Chem. Phys. Lett., submitted.
[37] X.W. Fan, K.T. Leung, J. Phys. B 34 (2001) 811.
[38] X.W. Fan, K.T. Leung, J. Chem. Phys. 115 (2001) 2603.
[39] X.W. Fan, K.T. Leung, Chem. Phys. Lett. 341 (2001) 638.
[40] J.F. Ying, T.A. Daniels, C.P. Mathers, H. Zhu, K.T. Leung, J. Chem. Phys. 99 (1993) 3390.
[41] J.W. Raymonda, L.O. Edwards, B.R. Russell, J. Am. Chem. Soc. 96 (1974) 1708.
[42] A.P. Hitchcock, C.E. Brion, J. Electron Spectrosc. Relat. Phenomen. 14 (1978) 417.
[43] M. Inokuti, J.L. Dehmer, T. Baer, J.D. Hanson, Phys. Rev. A 23 (1981) 95, and references therein.
[44] J.A. Wheeler, J.A. Bearden, Phys. Rev. 46 (1934) 755.
[45] J.F. Ying, Ph.D. Thesis, University of Waterloo, Waterloo (1994).
[46] S. Kasumata, K. Kimura, J. Electron Spectrosc. Relat. Phenomen. 6 (1975) 309.
[47] T. Ohta, H. Kuroda, Bull. Chem. Soc. Jpn. 49 (1976) 2939.
[48] W.B. Perry, W.L. Jolly, Inorg. Chem. 13 (1974) 1211.
[49] K. Imura, N. Kishimoto, K. Ohno, J. Phys. Chem. 105 (2001) 6378.
[50] T.N. Olney, G. Cooper, W.F. Chan, G.R. Burton, C.E. Brion, K.H. Tan, Chem. Phys. 205 (1996) 421.
[51] M.B. Robin, Higher Excited States of Polyatomic Molecules, Vol. 3, Academic, New York, 1985.